1 Background

Classical molecular dynamics simulations were performed to analyze the interface formed between various aqueous salt solutions and carbontetrachloride. Three salt solutions were simulated, as well as a reference system consisting of neat water for comparison to previous computational efforts.[1–6] The salts used in the simulations were NaCl, $NaNO_3$, and Na_2SO_4. These were chosen to compare to the experimental SFG results, and to supplement those experiments with additional molecular-level information. Analyses were performed on the simulation data to extract ionic and molecular density data, information about water coordination near to the interface, and water orientation data from order parameter analysis. The analyses are similar to, and logical extensions of previous computational work done on aqueous salt systems.

1.1 Density Profiles

Density histograms of simulated interfaces have been used in previous publications to show ionic and molecular distribution behavior in various systems.[2,4,6–11] In this work the density profile of water through the interface is fitted to a hyperbolic tangent function[10,12] as shown below:

$$\rho(z) = \frac{1}{2}(\rho_1 + \rho_2) - \frac{1}{2}(\rho_1 - \rho_2)\tanh\left(\frac{z - z_0}{d}\right) \tag{1}$$

Equation (1) relates the interfacial density, ρ, as a function of position, z, along a given system axis, to the densities of the phase on either side of the location of the Gibb's dividing surface, z_0. The bulk density ρ_1 and the density within the second phase, ρ_2 are fitted. The interfacial width, d, is related to the "90-10" thickness of the interface by:

$$t = 2.197d \tag{2}$$

These measures of interfacial thickness provide a means of comparing the depths to which the water phase is affected by ions located at the interface. The density distributions of the salts depict concentration and depletion phenomena throughout the interfacial region, and also serve to illustrate ionic affinity within this region. Previous work has been performed on the air-water interface with various ions introduced, showing varying levels of interfacial affinity, with the more polar ions being the most interfacially active. We present the density distribution results below for the neat-H_2O and salt solutions interfaced with an organic CCl_4 phase.

1.2 Molecular Orientation

Several computational methods have been used previously to show molecular orientation profiles of water molecules throughout interfacial regions.[?] In this work we have chosen to compute the orientation of water using two vectors that fully describe the orientation in space given the locations of the three atoms comprising

the molecule. The molecular bisector, a vector that points along the axis of symmetry of the water molecule from the hydrogen-end to the oxygen, gives the orientation of the molecule in an intuitive way. A second vector, what is refered to as the normal-vector, is established as the vector pointing normal to the plane formed by the three atoms of the water molecule and establishes the "tilt" of the molecule. Analyzing the angle made between these two vectors and a given space-fixed axis (the long axis of the system) is a means of finding the absolute orientation of waters within these simulated systems. The angle between the molecular bisector and the system Z-axis will hereafter be referred to as θ, and the molecular normal vector as ϕ. The analysis reported in this work shows the cosines of these two angles, and because of the symmetry of the water molecule where the hydrogens are not uniquely identified, the cosines of the two angles are limited as follows: $-1 \leq \theta \leq 1$ and $0 \leq \phi \leq 1$.

1.3 Radial Distribution Functions

In studying the water structure near to the interface with an organic phase, the radial distribution functions (RDF) for the water atoms were computed lending another metric of water's structure. The RDF's, $g(r)$, for each system were calculated and normalized to a gas-phase probability of unity at long distances, representing a complete loss of orientational correlation.

1.4 Computational SFG

2 Computational Setup

The molecular dynamics methods used in this work are similar to those from our previous computational efforts with some modifications described below.[1,2,4] Simulations were carried out using the Amber 9 software package. The polarizable molecular model parameters are taken from previous works on similar systems.[7,13–16] The polarizable POL3 model was used for water molecules.[17] Fully polarizable models have been used in previous interface simulation studies because they are known to more accurately reproduce interfacial structure and free energy profiles.[18–21]

A total of 4 systems were simulated consisting of aqueous salt and CCl_4 phases. A slab geometry was used to produce two interface regions, the analyses of which were averaged.[1] The organic region was formed in a box 30-Å on a side with 169 CCl_4 molecules to reproduce standard temperature density of 1.59-$\frac{g}{mL}$. The aqueous region was formed in a box 30x30x60-Å, with the long axis labeled the z-axis. The number of water molecules and ions varied for each system in order to reproduce a density of 1.2-M. The specific populations of each molecule are listed in table 2. The organic and aqueous boxes were then joined to form a system 90-Å long with interface areas of 30x30-Å.

System	H_2O	Cation	Anion
Neat Water	1800	0	0
NaCl	1759	40	40
$NaNO_3$	1732	40	40
Na_2SO_4	1740	86	43

Table 1 — Aqueous molecule and ion numbers. Listed are the populations of each component for the 4 simulated aqueous phases. All systems were simulated at near 1.2-M salt concentrations.

The water, salts, and CCl_4 were each randomly packed into their respective boxes with a minimum packing distance of 2.4-Å. After joining the aqueous and organic phases and forming the two interfaces, the total system was energy minimized using a conjugate gradient method. Following minimization, the system was equilibrated at a constant temperature of 298-K with weak coupling to a heat bath for a period of 10-ns, using a simulation timestep of 1.0-fs. A non-bonded potential cutoff of 9.0-Å was used. Following equilibration the system was simulated with the same parameters for a further 10-ns with atomic position data recorded every 50-fs. This resulted in a total of 200,000 snapshots which were used in the data analysis.

3 Component Densities

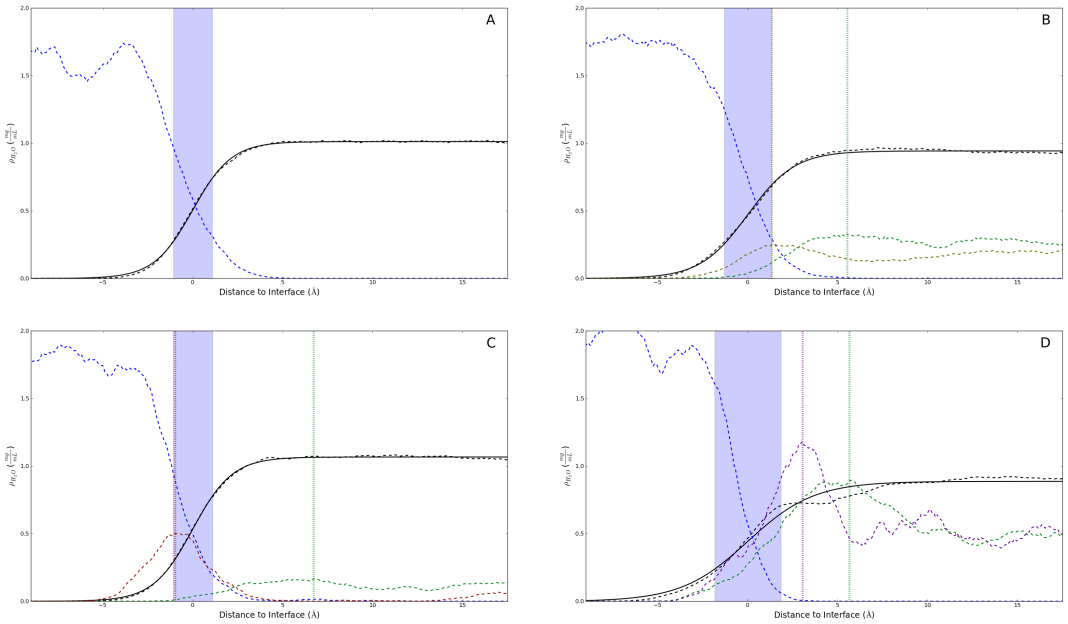

Figure. 1 — Aqueous salt and CCl_4 density profiles. The gibbs dividing surface location, z_0, were designated as the 0.0 $\mathring{A}$ location, and all lineshapes are plotted as distances to the gibbs interface. Neat-H_2O (A), NaCl (B), $NaNO_3$ (C), and Na_2SO_4 (D) salt-system densities are plotted with the water-oxygen density (dashed black) and the corresponding fitted lineshape (solid black). Each interfacial width, d, is designated as a highlighted blue region of width d centered about z_0. The CCl_4 (dashed blue), Na^+ cation (dashed green) and respective anion densities are also shown for each system. The scaling of the cation (10x) and anion (5x) densities was used to clarify their peak and trough locations. The maxima of the ionic components are marked with dashed vertical lines of the same colors to show relative component locations within the interfacial region.

The component density profiles of each system were calculated to study the effects of adding salts and to find deviations from the neat-H_2O/CCl_4 system. The water density profile of each system was fitted to a hyperbolic tangent (Eq. 1), and the all the density profiles were plotted as distances from each of the gibbs dividing surface locations, z_0. The resulting plots are shown in figure 1 with letter labels that will be used to refer to the systems. z_0 of each system was shifted to a location of 0.0 $\mathring{A}$, and the interfacial thickness, d, is visualized by a blue shaded region of the respective thickness centered about z_0. The widths of the interfacial regions for the neat-H_2O (A), NaCl (B), $NaNO_3$ (C), and Na_2SO_4 (D) systems are 2.16, 2.62, 2.20, and 3.69 $\mathring{A}$ respectively. In each of the salt solutions, the peak in the anionic density profile occurs closer to the CCl_4 phase than the corresponding cationic peak. Various parameters of interest such as the

interfacial thicknesses, ionic component locations, and relative distances between the peaks of the ion profiles are collected in table 2.

System	d	Anion	Cation	Anion-Cation Distance
Neat-H_2O	2.16	-	-	-
NaCl	2.62	1.33	5.53	4.20
$NaNO_3$	2.20	-0.99	6.71	7.70
Na_2SO_4	3.69	3.04	5.64	2.60

Table 2 — Aqueous salt system density parameters. Interfacial widths, d, and the locations of the maxima of the density profiles for each ionic component are listed for the simulated salt systems. The relative distances between the anion and cation density peak locations are listed to show how the different anions affect the relative location of their cationic counterions.

The oscillations in the surface density profiles of water and the adjoining organic liquid phase have been noted previously and attributed to thermal capillary waves on a larger length-scale than the simulated system size.[22] The same work also made note that the interfacial thickness is size-dependent on the interfacial surface area. Increasing the surface area dimensions should cause an increase in the interfacial width. Two works on the water-CCl_4 surface offer direct comparison of this.[2,22] In comparing the interfacial widths, there is an increase in width as the system cross-sectional area is increased. This phenomenon implies that care must be taken when making quantitative comparisons between simulation studies.

System A is the acting benchmark and has been simulated previously by various groups. Deviations in width of the interface from the pure-water system can be attributed to the added ions in the solution. In comparing the three salt solutions, any differences in those systems are anionic in nature because the cation of each system was kept the same. System B is the simplest of the three salts with a monatomic and monovalent anion. The peak of the anion density profile is within the aqueous phase and is found on the aqueous-side of the interfacial width, d. The location of the cation density peak is, as mentioned above, deeper into the aqueous phase than the anion by over 4 $\mathring{A}$. This layering of ions within the aqueous phase is attributed to the break in the anisotropy of the field of the bulk region upon introduction of the second (organic) phase. The more polarizable and negatively charged anions move towards the interface to effectively screen the charge of the second phase and the more highly ordered water structure. The counterions then are drawn towards the negative charge built up by the anions to create the second ion density peak. The overall shape of the water profile in system B is relatively unaffected as the bulk water density is unchanged, and the width of the interface is increased by 18% from that of system A.

System C introduces the monovalent, polyatomic nitrate anion. The location preference of nitrate is a contentious subject that has been studied much in recent years. Experimental works have been performed using a few surface-sensitive techniques. One work used sum frequency generation (SFG), which detected structural changes in the hydrogen-bonding network in the presence of the anion that affect the SFG signal intensity from the interface, but could not create the anion density profile[23]. The same work found SFG

intensity enhancement for hydrogen-bonded water following a trend of $H_2SO_4 \geq HCl > HNO_3$. Strengthening of the interfacial hydrogen-bonding structure of water would allow it to further penetrate into a second phase, thus widening the interface region, and enhancing the SFG intensity from the interface for hydrogen-bonded species. We find the same trend when comparing interfacial widths from our simulations. In the case of the nitrate anion location, however, the SFG studies stopped short of reporting a concentration profile. A recent X-ray photoemission spectroscopy study was performed to specifically determine the nitrate concentration profile for the water-vapor interface, and reported the current differences of opinion between recent experiment and simulation.[24] The XPS results reported a surface depletion of the nitrate anion relative to the bulk, similar to previous MD simulations of the same systems. Other works find similar nitrate surface depletions,[25] but were performed on the liquid-vapor interface, and help to contrast the effect of the presence of an organic phase as in the present work. We find a surface enhancement of the nitrate anion located far to the organic side of the interface. The nitrate density peak is located the furthest out from the aqueous phase of the three salt systems. The location of the sodium cation peak is a significant distance further into the bulk from the anion than either of systems B and D. Such surface location and enhancement of the nitrate ion suggests a very strong interaction with the interface waters, breaking the hydrogen-bonding network near to the organic phase, and also strongly screening the field of the CCl_4 molecules from the interface. This accounts for the narrower interfacial width as the water can no longer extend a bonded network into the organic phase. However, as the water is strongly interacting with the nitrate and effectively screening the surface charge from the bulk, the cation is less attracted to the interface and the ionic double-layer is widened. Xu, et al, studied this phenomena finding a lack of ion-pairing of various nitrates at the air-water interface.[26] They found that solvation from an abundance of water at the interface weakens coulombic forces between ions, leading to greater cation-anion separation. They concluded that the surface nitrate is dehydrated, and the water provides adequate shielding of the ionic coulombic interactions. It is reasonable to assume that this same effect may cause the greater cation-anion separation at the interface of system C, even in the presence of the organic phase.

The widest interface is that of the $NaSO_4$ solution in system D, indicating that the SO_4^{2-} ions act to affect the hydrogen bonding network between the surface waters. The location of the sulfate density enhancement is the furthest into the aqueous bulk of the three anions, and the divalent and highly polarizable nature of the anion appears to attract the counterion closest for the narrowest sub-surface ionic double-layer. This attraction is likely coulombic, and the charge screening that separates the ion pairs in system C is not present in system D. Although the geratest concentration enhancement is further into the bulk region, seemingly outside the region designated by the width, the water network is still greatly enhanced. This has been verified by an increase in SFG response of the surface waters relative to the neat-water system in a recent work by this group[27]

Most of the recent studies on ion concentration near water interfaces have noted that large and polarizable ions will concentrate at the surface,[8,20,28,29] while small non-polarizable ion tend to be repelled. The surface enhancement calculated from molecular dynamics, however, portrays the lower bound of the actual

effect because of the reduced polarizability values used in simulations to avoid the so-called "polarization catastrophe." The enhancement of surface anions is also believed to be the cause of the subsurface cation density increase. The counterions are attracted to the concentrations of anions at the surface, which are in turn stabilized by the increased polarization of the water due to the distorted interfacial electric field. The affinity for the surface follows the trend of surface tension increments, $\frac{d\gamma}{dm_2}$, where $Na_2SO_4 > NaCl > NaNO_3$.[28] This also follows the hoffmeister series trend for anions found to be the most "structure-making", and they are found to be enhanced further into the interface.

4 Water Orientation

5 Water Orientational Order Parameters

6 Calculated Sum-Frequency Spectra

References

1. Hore, D. K.; Walker, D. S.; MacKinnon, L.; Richmond, G. L. *Journal of Physical Chemistry C* **2007,** *111,* 8832-8842.

2. Hore, D. K.; Walker, D. S.; Richmond, G. L. *Journal of the American Chemical Society* **2008,** *130,* 1800+.

3. Hore, D. K.; Walker, D. S.; Richmond, G. L. *Journal of the American Chemical Society* **2007,** *129,* 752-753.

4. Walker, D. S.; Hore, D. K.; Richmond, G. L. *Journal of Physical Chemistry B* **2006,** *110,* 20451-20459.

5. Walker, D. S.; Richmond, G. L. *Journal of the American Chemical Society* **2007,** *129,* 9446-9451.

6. Walker, D. S.; Moore, F. G.; Richmond, G. L. *Journal of Physical Chemistry C* **2007,** *111,* 6103-6112.

7. Chang, T.; Peterson, K.; Dang, L. *Journal of Chemical Physics* **1995,** *103,* 7502-7513.

8. Eggimann, B. L.; Siepmann, J. I. *Journal of Physical Chemistry C* **2008,** *112,* 210-218.

9. Du, H.; Liu, J.; Ozdemir, O.; Nguyen, A. V.; Miller, J. D. *Journal of Colloid and Interface Science* **2008,** *318,* 271-277.

10. Wick, C.; Dang, L. *Journal of Physical Chemistry B* **2006,** *110,* 6824-6831.

11. Petersen, P.; Saykally, R.; Mucha, M.; Jungwirth, P. *Journal of Physical Chemistry B* **2005,** *109,* 10915-10921.

12. MATSUMOTO, M.; KATAOKA, Y. *Journal of Chemical Physics* **1988,** *88,* 3233-3245 hyperbolic tangent fitting function for water density profiles.

13. Chang, T.; Dang, L. *Journal of Physical Chemistry B* **1997,** *101,* 10518-10526.

14. Dang, L. *Journal of Physical Chemistry B* **1999,** *103,* 8195-8200.

15. Thomas, J. L.; Roeselova, M.; Dang, L. X.; Tobias, D. J. *Journal of Physical Chemistry A* **2007,** *111(16),* 3091-3098.

16. Hrobarik, T.; Vrbka, L.; Jungwirth, P. *BIOPHYSICAL CHEMISTRY* **2006,** *124,* 238-242.

17. Caldwell, J. W.; Kollman, P. A. *J. Phys. Chem.* **1995,** *99,* 6208-6219.

18. Rivera, J. L.; Starr, F. W.; Paricaud, P.; Cummings, P. T. *JOURNAL OF CHEMICAL PHYSICS* **2006,** *125,*.

19. Wick, C. D.; Kuo, I.-F. W.; Mundy, C. J.; Dang, L. X. *Journal of Chemical Theory and Computation* **2007,** *3,* 2002-2010.

20. Petersen, P.; Saykally, R. *Journal of the American Chemical Society* **2005,** *127,* 15446-15452.

21. Dang, L. *Journal of Physical Chemistry B* **1998,** *102,* 620-624.

22. Chang, T.; Dang, L. *Journal of Chemical Physics* **1996,** *104,* 6772-6783.

23. Schnitzer, C.; Baldelli, S.; Shultz, M. *JOURNAL OF PHYSICAL CHEMISTRY B* **2000,** *104,* 585-590.

24. Brown, M. A.; Winter, B.; Faubel, M.; Hemminger, J. C. *JOURNAL OF THE AMERICAN CHEMICAL SOCIETY* **2009,** *131,* 8354+.

25. Otten, D. E.; Petersen, P. B.; Saykally, R. J. *Chemical Physics Letters* **2007,** *449,* 261-265.

26. Xu, M.; Tang, C. Y.; Jubb, A. M.; Chen, X.; Allen, H. C. *JOURNAL OF PHYSICAL CHEMISTRY C* **2009,** *113,* 2082-2087.

27. McFearin, C. L.; Richmond, G. L. *JOURNAL OF PHYSICAL CHEMISTRY C* **2009,** *113,* 21162-21168.

28. Pegram, L. M.; Record, Jr., M. T. *PROCEEDINGS OF THE NATIONAL ACADEMY OF SCIENCES OF THE UNITED STATES OF AMERICA* **2006,** *103,* 14278-14281.

29. Sloutskin, E.; Baumert, J.; Ocko, B. M.; Kuzmenko, I.; Checco, A.; Tamam, L.; Ofer, E.; Gog, T.; Gang, O.; Deutsch, M. *JOURNAL OF CHEMICAL PHYSICS* **2007,** *126,*.